Jiang et al. Nanoscale Research Letters (2018) 13:301
https://doi.org/10.1186/s11671-018-2719-7

Nanoscale Research Letters

NANO EXPRESS Open Access

First-Principles Study of Point Defects in GaAs/AlAs Superlattice: the Phase Stability and the Effects on the Band Structure and Carrier Mobility

Ming Jiang[1], Haiyan Xiao[1*], Shuming Peng[2], Liang Qiao[1], Guixia Yang[2], Zijiang Liu[3] and Xiaotao Zu[1]

Abstract

Advanced semiconductor superlattices play important roles in critical future high-tech applications such as aerospace, high-energy physics, gravitational wave detection, astronomy, and nuclear related areas. Under such extreme conditions like high irradiative environments, these semiconductor superlattices tend to generate various defects that ultimately may result in the failure of the devices. However, in the superlattice like GaAs/AlAs, the phase stability and impact on the device performance of point defects are still not clear up to date. The present calculations show that in GaAs/AlAs superlattice, the antisite defects are energetically more favorable than vacancy and interstitial defects. The As_X (X = Al or Ga) and X_{As} defects always induce metallicity of GaAs/AlAs superlattice, and Ga_{Al} and Al_{Ga} antisite defects have slight effects on the electronic structure. For GaAs/AlAs superlattice with the interstitial or vacancy defects, significant reduction of band gap or induced metallicity is found. Further calculations show that the interstitial and vacancy defects reduce the electron mobility significantly, while the antisite defects have relatively smaller influences. The results advance the understanding of the radiation damage effects of the GaAs/AlAs superlattice, which thus provide guidance for designing highly stable and durable semiconductor superlattice based electronic and optoelectronics for extreme environment applications.

Keywords: Hybrid density functional theory, Point defect, GaAs/AlAs superlattice, Electrical properties

Background

The superlattice (SL) is an artificial material consisting of alternating thin layers of two or more different components. The $(GaAs)_n/(AlAs)_m$ is one of the most important SL since the development of high electron mobility transistors (HEMT) and quantum cascade lasers (QCLs) a few decades ago [1–6]. Recently with the advances of film epitaxy and nanofabrication techniques, the $(GaAs)_n/(AlAs)_m$ based SLs and nanodevices with (n + m) ranging from 2 to 10 have demonstrated exciting physical properties related to luminescence and optical absorption, two-phonon absorption, and Raman as well as infrared spectra, which thus found promising applications in optoelectronics, sensing, LED, energy and laser related civilian and industrial areas [7–12]. Meanwhile, toward other critical high-tech applications such as aerospace, high-energy physics, gravitational wave detection, astronomy, space travel, nuclear and national security related areas, the semiconductor SLs and devices are exposed to different radiation environments, i.e., X-ray, neutrons, electrons, ions, etc., which may result in the generation of defects containing impurities, vacancies, interstitials, antisites, and complex of these. Since the semiconductor materials and related physical properties play an important role in operating and functioning these electronic devices and integrated circuits, small amounts of defects may drastically change their optical and transport properties, especially in multilayer systems [13].

The effects of foreign impurities or intrinsic defects on the semiconductor SLs and their component materials have been extensively investigated in the past decades.

* Correspondence: hyxiao@uestc.edu.cn
[1]School of Physics, University of Electronic Science and Technology of China, Chengdu 610054, China
Full list of author information is available at the end of the article

Zollo et al. have employed density functional theory (DFT) method to investigate the stability of point defects in GaAs, and found that the antisite defects were more favorable [14]. Kahaly et al. have studied GaAs/AlAs SL structure by DFT method and found the arsenic vacancy (V_{As}) defect at and near the interface led to a conducting quasi 2-DEG between insulating dielectric arsenide [7]. Spasov et al. have studied the effects of nitrogen impurities on carrier transport and electron-hole recombination in GaAs/AlAs SL diodes [9]. They reported that the N impurities modified the energy of the electronic miniband and impeded electron diffusion through the SL miniband, which may lead to a strong radiative recombination of electron-hole pairs [9]. Wang et al. studied the inter-diffusion induced by the Zn impurity in GaAs/AlAs SL structures employing an *ab initio* molecular dynamics (AIMD) method [15]. Their results suggested that the Zn diffusion was assisted by the group-III elements, which were ejected into the interstitial channel and diffused rapidly, thereby disordering the superlattice [15]. Mitra and Stark found that the presence of vacancies enhanced the Ga/Al intermixing in GaAs/AlAs SL, resulting from the proposed two-atom ring mechanism of diffusion [16]. Recently, an AIMD simulation of radiation response of GaAs/AlAs SL has been carried out [17], in which the minimum energies for each atom to be permanently displaced from its lattice site have been determined, the pathways for defect generation have been provided, and the types of created defects have been identified. It revealed that the created Ga (or Al or As) Frenkel pair and As_{Ga}-Ga_{As} antisite pair have profound effects on the density of state distribution and band structure of GaAs/AlAs SL [17].

So far, the stability of point defects in SL structure and the transport properties like carrier mobility still remain unknown. It is thus of vital importance to investigate how the presence of vacancy, interstitial and antisite defects influences the structural stability and electrical properties of GaAs/AlAs SL. In this study, the phase stability of single Ga (or Al or As) vacancy, single Ga (or Al or As) interstitial and single Ga_{As} (or Al_{As} or As_{Ga} or As_{Al}) antisite defects have been studied. It is shown that the antisite defects are energetically more favorable than vacancy and interstitial defects. The band structures of these defective states have been investigated by the hybrid DFT method, which incorporates a portion of exact exchange from Hartree–Fock theory with the rest of the exchange-correlation energy from other sources (*ab initio* or empirical) [18], and is expected to offer a more accurate description of electronic structure of semiconductor materials than the standard DFT. In particular, the electron mobility has been predicted. It turns out the interstitial and vacancy defects reduce the electron mobility significantly, while the antisite defects have relatively smaller influences. This work will advance the understanding of the radiation damage effects of the semiconductor superlattice and provide guidance for designing highly stable and durable semiconductor superlattices-based electronic and optoelectronics for extreme environment applications.

Methods

In this study, the structural relaxations are carried out within the standard DFT framework and the band structures are calculated by the hybrid DFT in the framework of Heyd-Scuseria-Emzefhof (HSE) [19] based on the relaxed structures. All calculations are carried out employing Vienna *Ab Initio* Simulation Package (VASP) [20]. Projector augmented-wave pseudopotentials are used to describe the interaction between ions and electrons, and the exchange-correlation effects are treated using the local density approximation in the Ceperley-Alder parameterization [21]. The convergence criteria for total energies and forces are 10^{-4} eV and 10^{-3} eV/Å, respectively. The origin point group of AlAs and GaAs crystal is the T_d group of zinc blende, as shown in Fig. 1a. The illustration of considered point defects is provided in Fig. 1b. The GaAs/AlAs SL containing two monolayers of GaAs alternating with two monolayers of AlAs is considered in this study and the geometrical configuration is illustrated in Fig. 2, together with the considered point defects.

Results and Discussion

Ground State Properties of GaAs and AlAs

As shown in Table 1, the lattice constants of bulk GaAs and AlAs are determined to be 5.61 and 5.63 Å, respectively, which agree well with the experimental and other theoretical values [22–24]. It seems that the lattice mismatch between GaAs and AlAs is small, and the lattice constant of GaAs/AlAs SL is set to be the intermediate value of 5.62 Å. The bulk modulus is calculated by $B = \frac{1}{3}(C_{11} + 2C_{12})$ [25], where the C_{11} and C_{12} represent the elastic constants. The bulk modulus of GaAs is calculated to be 76.3 GPa, which is close to the result of 76.5 GPa for AlAs. These results are in reasonable agreement with the theoretical and experimental data [22, 26, 27].

The Defect Formation Energy in GaAs/AlAs Superlattice

For GaAs/AlAs SL and bulk states, the defect formation energy is calculated by $E_f = E_{def} - E_{undef} + \sum_i \Delta n_i \mu_i$ [28]. Here, E_{def} is the total energy of the defective simulation cell after relaxation, E_{undef} is the total energy of the relaxed ideal supercell, Δn_i is the change in the

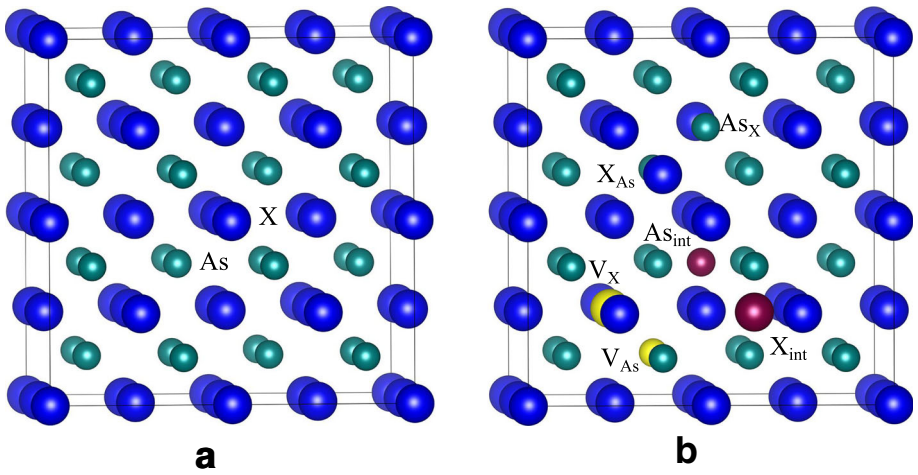

Fig. 1 Schematic view of geometrical structures of **a** XAs (X = Ga or Al); **b** the defects in XAs. V_X: (X = Ga, Al, or As) X vacancy; X_{int}: X interstitial; X_{As}: X occupying the As lattice site; As_X: As occupying the X lattice site. The yellow and purple spheres represent the vacancy and interstitial defects, respectively

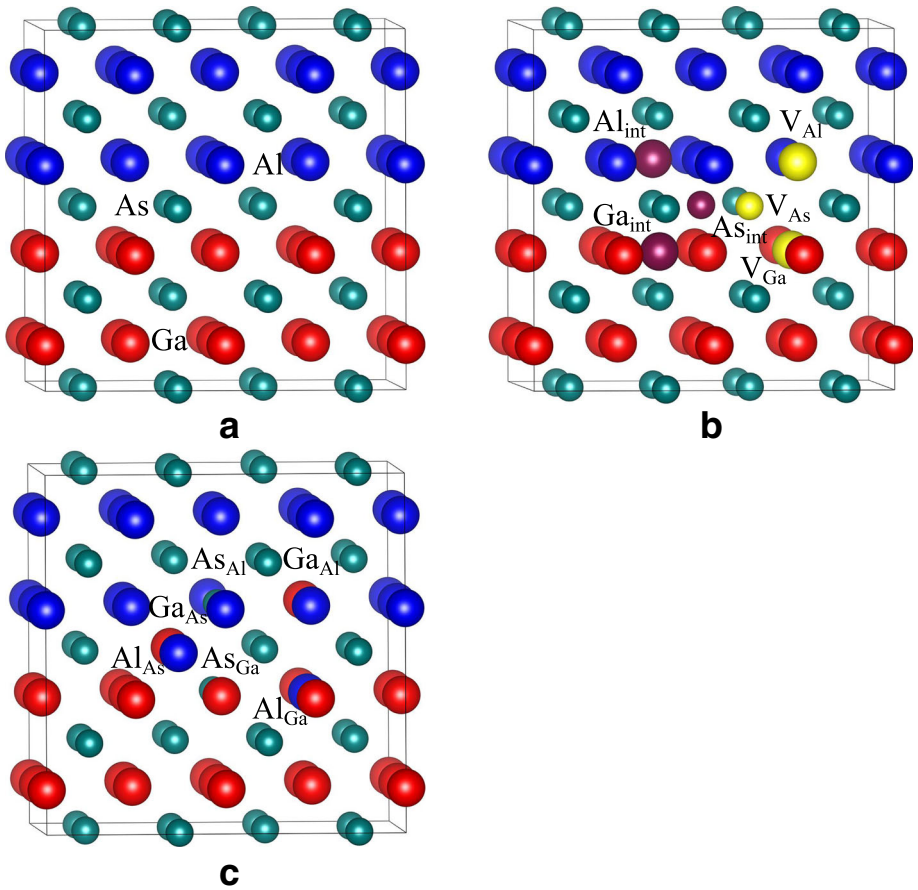

Fig. 2 Schematic view of geometrical structures of **a** ideal GaAs/AlAs superlattice; **b** and **c** GaAs/AlAs superlattice with different point defects. X_Y: (X, Y = Ga, Al, or As) X occupying the Y lattice site; V_X: X vacancy; X_{int}: X interstitial. The yellow and carmine spheres represent the vacancy and interstitial defects, respectively

Table 1 The calculated and experimental ground state properties of bulk GaAs and AlAs. The a_0 and B refer to the lattice constant and bulk modulus, respectively

	a_0 (Å)	B (GPa)
GaAs		
Our Cal.	5.61	76.3
Other Cal.	5.61[a]	75.2[a]
Exp.	5.65[b]	76[c]
AlAs		
Our Cal.	5.63	76.5
Other Cal.	5.63[a]	75.1[a]
Exp.	5.66[d]	77.3[e]

[a]Ref. [22]
[b]Ref. [24]
[c]Ref. [27]
[d]Ref. [23]
[e]Ref. [26]

number of species i (i = Ga, Al, or As), and μ_i is the chemical potential of species i [28].

For bulk XAs (X = Al or Ga), the chemical potentials of As and X obey the following constrains: $\mu_X \leq \mu_X^{bulk}$, $\mu_{As} \leq \mu_{As}^{bulk}$, and $\mu_{As} + \mu_X = \mu_{XAs}^{bulk}$, where μ_X^{bulk}, μ_{As}^{bulk}, and μ_{XAs}^{bulk} correspond to the total energy of bulk X, bulk As and bulk XAs, respectively. The defect formation energies under X-rich condition, i.e., $\mu_X = \mu_X^{bulk}$ and $\mu_{As} = \mu_{XAs}^{bulk} - \mu_X^{bulk}$, and As-rich condition, i.e., $\mu_{As} = \mu_{As}^{bulk}$ and $\mu_X = \mu_{XAs}^{bulk} - \mu_{As}^{bulk}$, are summarized in Table 2. For GaAs, under As-rich conditions the As_{Ga} (As occupying the Ga lattice site) antisite defect is found to be the most energetically favorable, as indicated by the smallest formation energy of 1.57 eV. The next favorable defect is the Ga_{As} (Ga occupying the As lattice site) antisite defect, with the formation energy of 2.31 eV. The As interstitial (As_{int}) has the largest formation energy of 5.20 eV, suggesting that it is more difficult to form than other considered point defects. Under Ga-rich conditions, the V_{Ga}, As_{int} and As_{Ga} defects have larger formation energies, and the V_{As}, Ga_{int} and Ga_{As} defects have smaller formation energies, as compared with the As-rich condition. Obviously, the defect stability depends on the chemical environment. As compared with GaAs, the defect formation energies in AlAs are generally larger, except the cases of As_{int} and As_X (X = Al or Ga) under As-rich conditions. The As_{Al} and Al_{As} antisite defects are determined to be the most favorable defect under As-rich and Al-rich conditions, respectively. Similar to the case of GaAs, the As_{int} is also unfavorable in AlAs. The defect formation energies under As-rich and X-rich (X = Ga or Al) conditions in bulk XAs are plotted in Fig. 3. Figure 3a shows that the As_{Ga} and Ga_{As} antisite defects are more favorable under As-rich and Ga-rich conditions, respectively. It is noted that the As_{Al} antisite defect is preferable in most cases (see Fig. 3b). Under Al-rich condition, the phase stability of Al_{As}, V_{As} and As_{Al} defects are close to each other, as indicated by the formation energies of 3.0, 3.16 and 3.24 eV, respectively. Also, we find that in both GaAs and AlAs, the non-favorability of As_{int} is independent of the chemical environment. Zollo et al. carried out first-principles calculations on GaAs and their DFT results showed that the formation energies of As_{Ga} and Ga_{As} were smaller than those for vacancy and interstitial defects [14], which are consistent with our results.

Table 2 The calculated defect formation energies (eV) in bulk XAs (X = Al or Ga) under As-rich and X-rich conditions. The minimum values are indicated in italic

Defect	GaAs		AlAs	
	As-rich	Ga-rich	As-rich	Al-rich
V_X	2.56	3.17	3.36	4.25
V_{As}	3.31	2.7	4.05	3.16
X_{int}	3.23	2.61	4.33	3.44
As_{int}	5.20	5.81	5.14	6.03
X_{As}	2.31	*1.49*	4.78	*3.0*
As_X	*1.57*	2.79	*1.46*	3.24

V_X: (X = Ga, Al, or As) X vacancy; X_{int}: X interstitial; X_{As}: X occupying the As lattice site; As_X: As occupying the X lattice site

The E_f in GaAs/AlAs SL structure are also calculated under As-rich condition, i.e., $\mu_{As} = \mu_{As}^{bulk}$, $\mu_{Al} = \mu_{AlAs}^{bulk} - \mu_{As}^{bulk}$, and $\mu_{Ga} = \mu_{GaAs}^{bulk} - \mu_{As}^{bulk}$, and cation-rich condition, i.e., $\mu_{Al} = \mu_{Al}^{bulk}$, $\mu_{Ga} = \mu_{Ga}^{bulk}$ and $\mu_{As} = (\mu_{SL}^{bulk} - n_{Al} \times \mu_{Al}^{bulk} - n_{Ga} \times \mu_{Ga}^{bulk})/n_{As}$, where n_{Al}, n_{Ga}, and n_{As} represent the number of Al, Ga and As atoms in the simulation cell, respectively. As shown in Table 3, the Al_{Ga} defect has negative formation energies, i.e., – 0.62 and – 0.27 eV under As-rich and cation-rich conditions, respectively, indicating that the formation of Al_{Ga} antisite defect is an exothermic process. As for Ga_{Al} defect, the formation energies are as small as – 0.01 eV under As-rich condition and 0.29 eV under cation-rich condition. Obviously, the formation of Al_{Ga} and Ga_{Al} antisite defects in the GaAs/AlAs SL structure are much easier than other point defects. Under As-rich condition, the formation energies of the second favorable defects of As_{Ga} and As_{Al} are determined to be 1.67 and 1.74 eV, respectively. For the interstitials, the phase stability both follows the trend of $Ga_{int} > Al_{int} > As_{int}$ under As-rich and cation-rich conditions. The defect formation energies in GaAs/AlAs SL structure are also plotted in Fig. 3c. As compared with the bulk GaAs, the point defects in GaAs/AlAs SL are

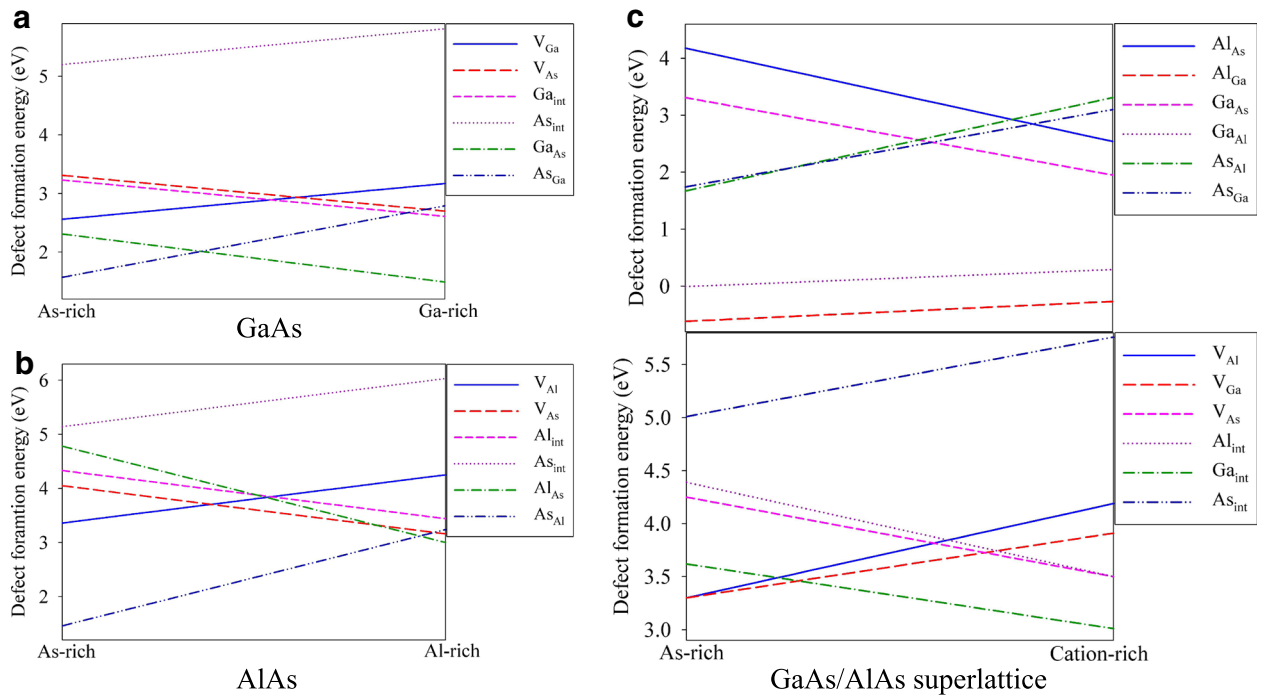

Fig. 3 The defect formation energies under As-rich and cation-rich conditions in **a** GaAs, **b** AlAs and **c** GaAs/AlAs superlattice. X_Y: (X, Y = Ga, Al, or As) X occupying the Y lattice site; V_X: X vacancy; X_{int}: X interstitial

Table 3 The calculated defect formation energies (eV) in GaAs/AlAs superlattice under cation-rich and As-rich conditions

Defect type	As-rich	Cation-rich
Antisite		
Ga_{Al}	− 0.01	0.29
Ga_{As}	3.31	1.95
Al_{Ga}	− 0.62	− 0.27
Al_{As}	4.18	2.54
As_{Ga}	1.67	3.31
As_{Al}	1.74	3.10
	Vacancy	
V_{Ga}	3.30	3.91
V_{Al}	3.30	4.19
V_{As}	4.25	3.50
	Interstitial	
Ga_{int}	3.62	3.01
Al_{int}	4.39	3.50
As_{int}	5.01	5.76

X_Y: (X, Y = Ga, Al, or As) X occupying the Y lattice site; V_X: X vacancy; X_{int}: X interstitial

generally more difficult to form, except the case of As_{int} (see Fig. 3a, c). The formation energies of As_{int} in bulk GaAs are 5.20 and 5.81 eV under As-rich and Ga-rich conditions, which are slightly larger than the corresponding values of 5.01 and 5.76 eV in GaAs/AlAs SL. As shown in Fig. 3b and c, the stability of point defects in bulk AlAs and SL structure shows different character. The Al_{As} and As_{int} defects are more energetically favorable in GaAs/AlAs SL than bulk AlAs, whereas V_{As} defect is more preferable in bulk AlAs than SL structure. It is noticeable that under As-rich and Al-rich conditions, the formation energies of Al_{int} in bulk AlAs are comparable to that in GaAs/AlAs SL. Similar to the case of Al_{int}, the V_{Al} defect in bulk AlAs and SL structure show similar favorability, as indicated by the comparable formation energies. In the case of As_{Al} defect, the formation energy under As-rich condition is smaller (1.46 eV) in SL structure, whereas under cation-rich condition, the value is smaller (3.10 eV) in bulk AlAs, suggesting that the stability of As_{Al} depends on the chemical environment.

Comparing the defect stability in bulk AlAs, GaAs and GaAs/AlAs SL, we find that the antisite defects are always more preferable than vacancies and interstitials, especially for the cases of Ga_{Al} and Al_{Ga} in GaAs/AlAs SL. It is also noted that under As-rich and cation-rich conditions, the As_{int} defect is the most difficult to form in both bulk states and GaAs/AlAs SL structure.

Table 4 The calculated band gap (eV) for bulk GaAs, AlAs, and GaAs/AlAs superlattice

	DFT	Hybrid DFT	Exp.
GaAs	0.50 (0.54[a])	1.44 (1.36[b])	1.52[c]
AlAs	1.31 (1.33[d])	2.16 (2.24[e])	2.22[f]
GaAs/AlAs SL	1.14 (1.16[g])	2.06	2.09[h]

[a]Ref. [8]
[b]Ref. [29]
[c]Ref. [24]
[d]Ref. [40]
[e]Ref. [41]
[f]Ref. [23]
[g]Ref. [3]
[h]Ref. [30]

The Effects of Point Defects on the Band Structures of GaAs/AlAs Superlattice

The Pristine State of GaAs/AlAs Superlattice

The band gaps for bulk GaAs, AlAs and GaAs/AlAs SL are summarized in Table 4, and their band structures are presented in Fig. 4. The hybrid DFT calculations determine the direct band gap of GaAs to be 1.44 eV (see Fig. 4a), which agrees well with the experimental value of 1.52 eV [29] and other calculations [24]. By contrast, the standard DFT predicts a band gap value of 0.5 eV, which largely underestimates the band gap of GaAs. For AlAs, the band structure is of indirect character and the hybrid DFT band gap is 2.16 eV (see Fig. 4b), which is 0.85 eV larger than the DFT result and in good agreement with the experimental value of 2.22 eV [23]. As shown in Fig. 4c, the band gap of GaAs/AlAs SL is determined to be direct and it is consistent with the study of Botti et al., who found the band gap of $(GaAs)_m/(AlAs)_m$ SL ($m \geq 2$) to be direct at the Γ point [3]. In our calculations, the direct band gap for GaAs/AlAs SL is determined to be 2.06 eV by hybrid DFT method, which is in agreement with the experimental value of 2.10 eV [30].

The Effects of Antisite Defects on the Band Structure of GaAs/AlAs Superlattice

In GaAs/AlAs SL structure, the Ga_{Al} and Al_{Ga} antisite defects are more energetically favorable than other point defects. As shown in Fig. 5a and b, the band structures of Ga_{Al} and Al_{Ga} defective states are very similar to that of the pristine state and the band gaps are determined to

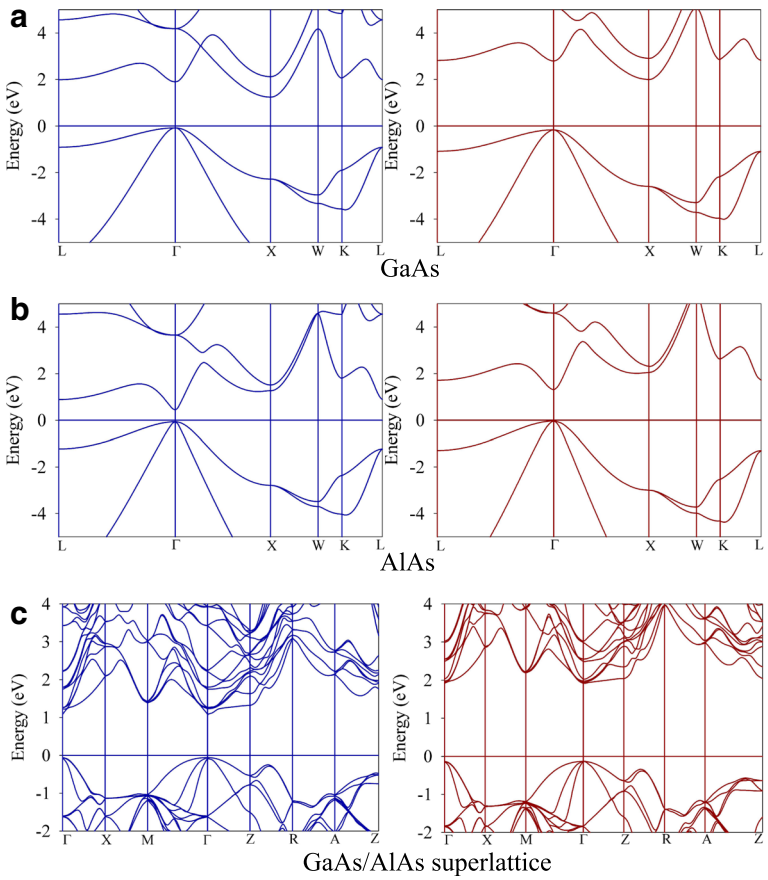

Fig. 4 The band structures of **a** GaAs, **b** AlAs and **c** GaAs/AlAs superlattice. The hybrid DFT values are plotted in left-hand panels and the DFT results are plotted in the right-hand panels

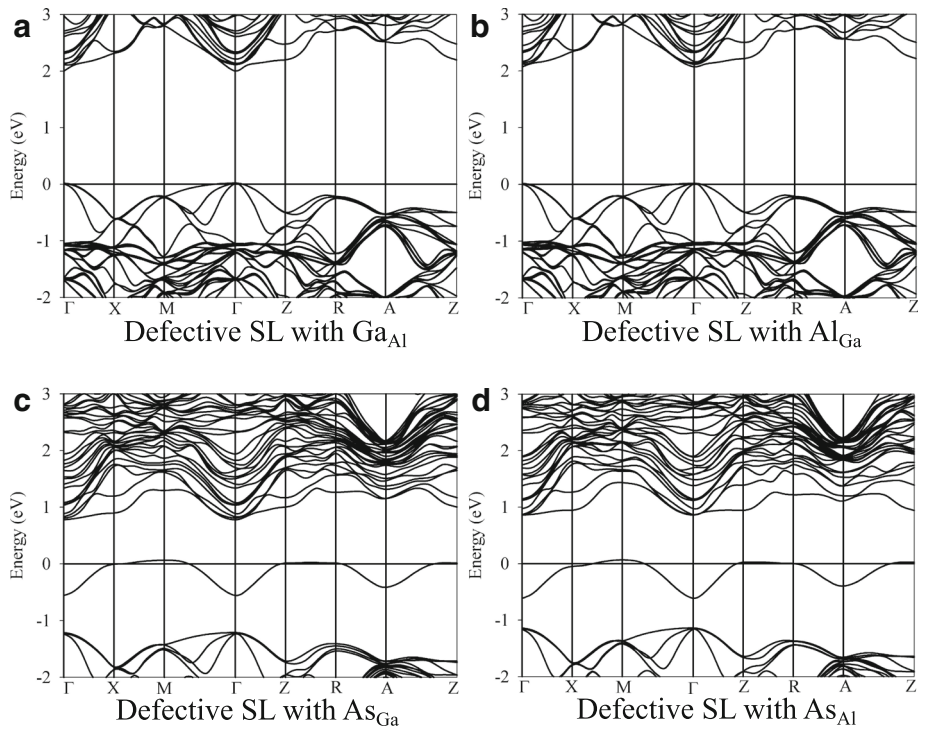

Fig. 5 The band structures of defective GaAs/AlAs superlattice with different antisite defects. **a**: Ga occupying the Al lattice site; **b**: Al occupying the Ga lattice site; **c**: As occupying the Ga lattice site; **d**: As occupying the Al lattice site

be 1.98 and 2.01 eV, respectively. This should be due to the fact that the Al and Ga chemical elements have similar valence electron configuration, i.e.,$3s^2 3p^1$ for Al and $4s^2 4p^1$ for Ga, and no extra electrons or holes are introduced upon the formation of Ga_{Al} and Al_{Ga} antisite defects. The band structures for As_{Ga} and As_{Al} defective states are depicted in the Fig. 5c and d. It turns out that these two defects modify the band structure of GaAs/AlAs SL considerably. Both the As_{Ga} and As_{Al} antisite defects introduce extra electrons and act as n-type dopants. The impurity levels are found to be far from the valence bands and cross the fermi level, as shown in Fig. 5c and d. These deep defect levels may act as the recombination center for carriers.

Figure 6 presents the band structures and partial density of state (PDOS) of defective SL with Ga_{As} and Al_{As} defects. As shown in Fig. 6a, the band structure for Ga_{As} defective SL is of spin splitting character. In the spin-down subbands, the fermi level passes through the defect levels introduced by the Ga_{As} defect, indicative of half-metallic character of the defective SL. According to the definition of half-metallic gap [31], the band gap of Ga_{As} defective state is about 0.10 eV. As shown in the PDOS of the defective SL with Ga_{As}, the spin-down subbands near the fermi level are mainly contributed by *p* partial waves. Due to the similar valence electron configurations between Ga and Al atoms, the calculated spin-up and spin-down band structures of Al_{As} defective state are determined (see Fig. 6b), and the band gap is calculated to be 0.15 eV. Overall, the Al_{Ga} and Ga_{Al} antisite defects have negligible effects on the electronic structure of GaAs/AlAs SL. It is also noted that the defective SL with As_{Al} and As_{Ga} defects show metallicity, while the defective SLs with Ga_{As} and Al_{As} are half-metallic.

The Effects of Vacancy Defects on the Band Structure of GaAs/AlAs Superlattice

The band structures of SL structure with different vacancies are plotted in the Fig. 7, and their corresponding PDOS are depicted in Fig. 8. The spin splitting character of band structure is also found in the case of defective SL with V_{Ga} and V_{Al} defects, as shown in Fig. 7a and b. Indeed, removal of atoms from their original positions leaves four dangling bonds related to the sp^3 orbitals. During the structural relaxation, the nearest atoms around the vacancy are equally displaced toward the empty lattice site, which results in site-symmetry defined by the tetragonal D_{2d} point group. The induced defect levels appear near the valence band and locate in the forbidden region of the GaAs/AlAs SL. The band gap is determined to be 0.47 and 0.44 eV for the SL with V_{Ga} and V_{Al} defects, respectively. As shown in the PDOS of defective SL with V_{Ga} and V_{Al} (see Fig. 8a and b), the

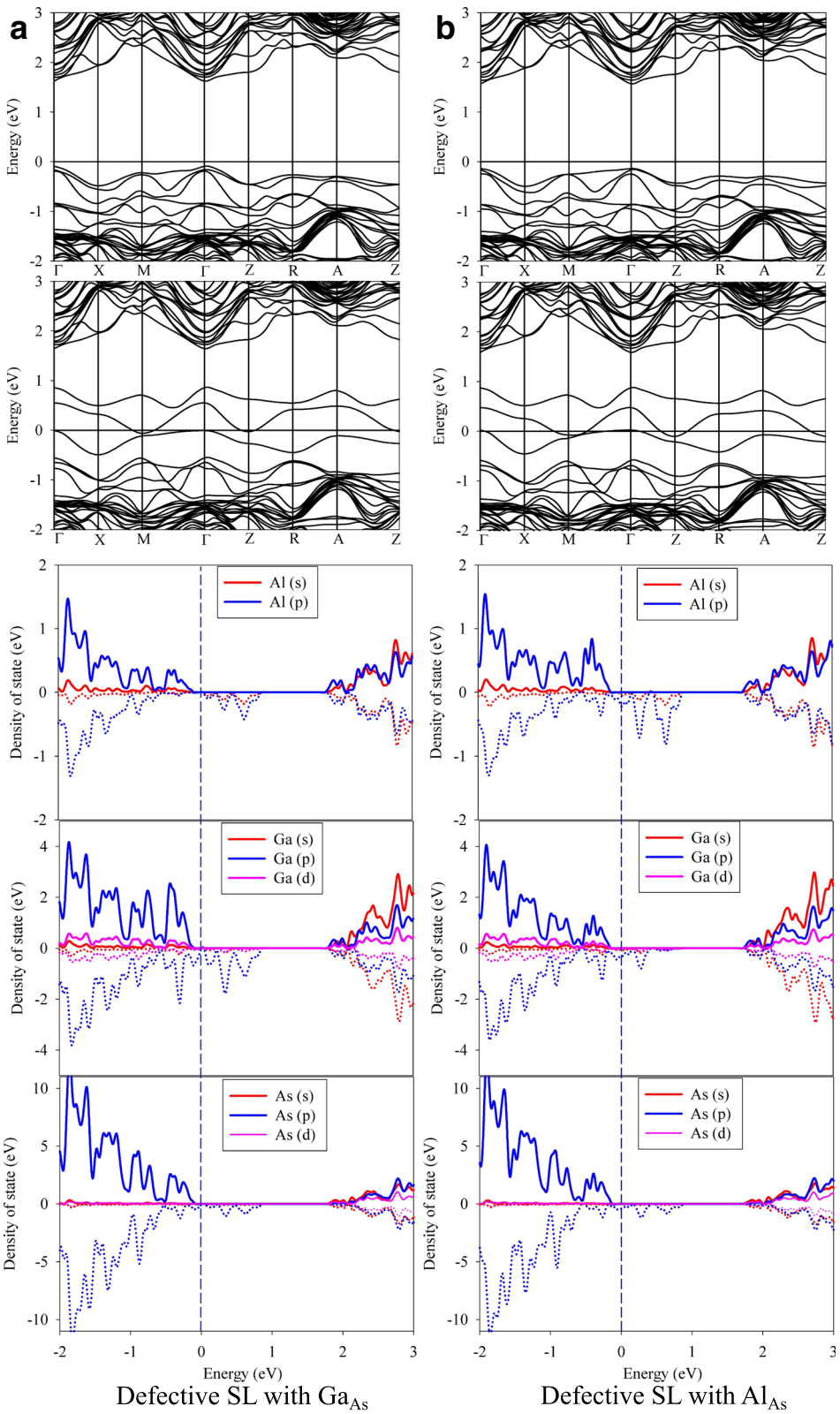

Fig. 6 The band structures and partial density of state of defective GaAs/AlAs superlattice with **a** Ga_{As} and **b** Al_{As} antisite defects. X_{As} (X = Ga or Al) X occupying the As lattice site

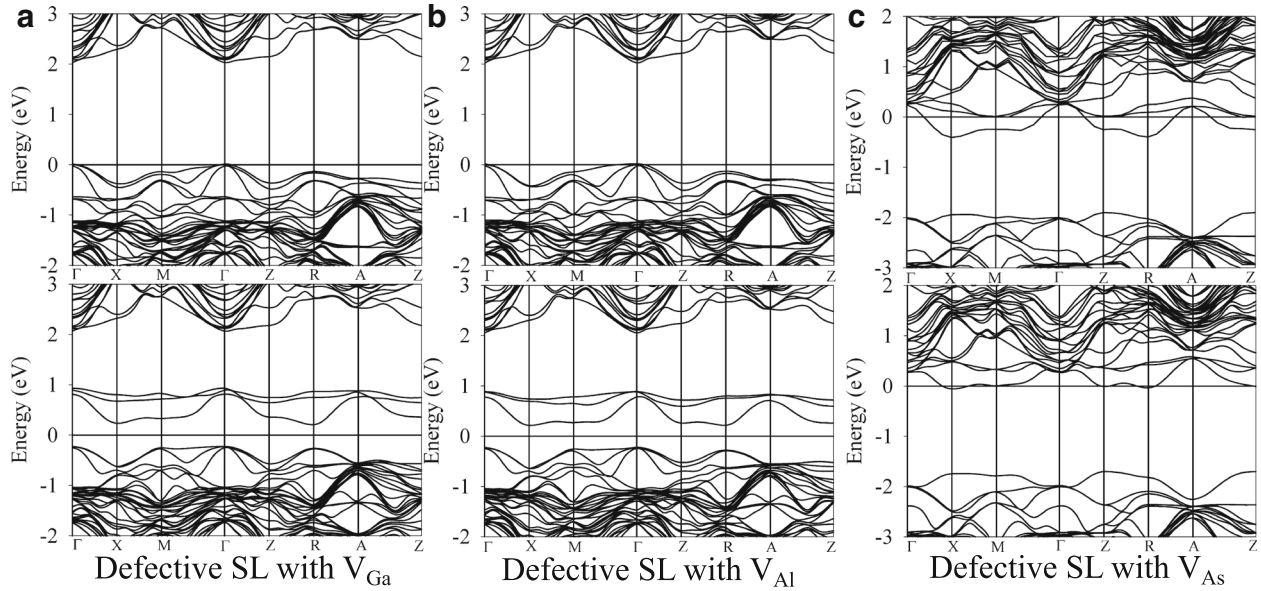

Fig. 7 The band structures of defective GaAs/AlAs superlattice with **a** V_{Ga}, **b** V_{Al} and **c** V_{As} vacancy defects. V_X (X = Ga, Al, or As) X vacancy

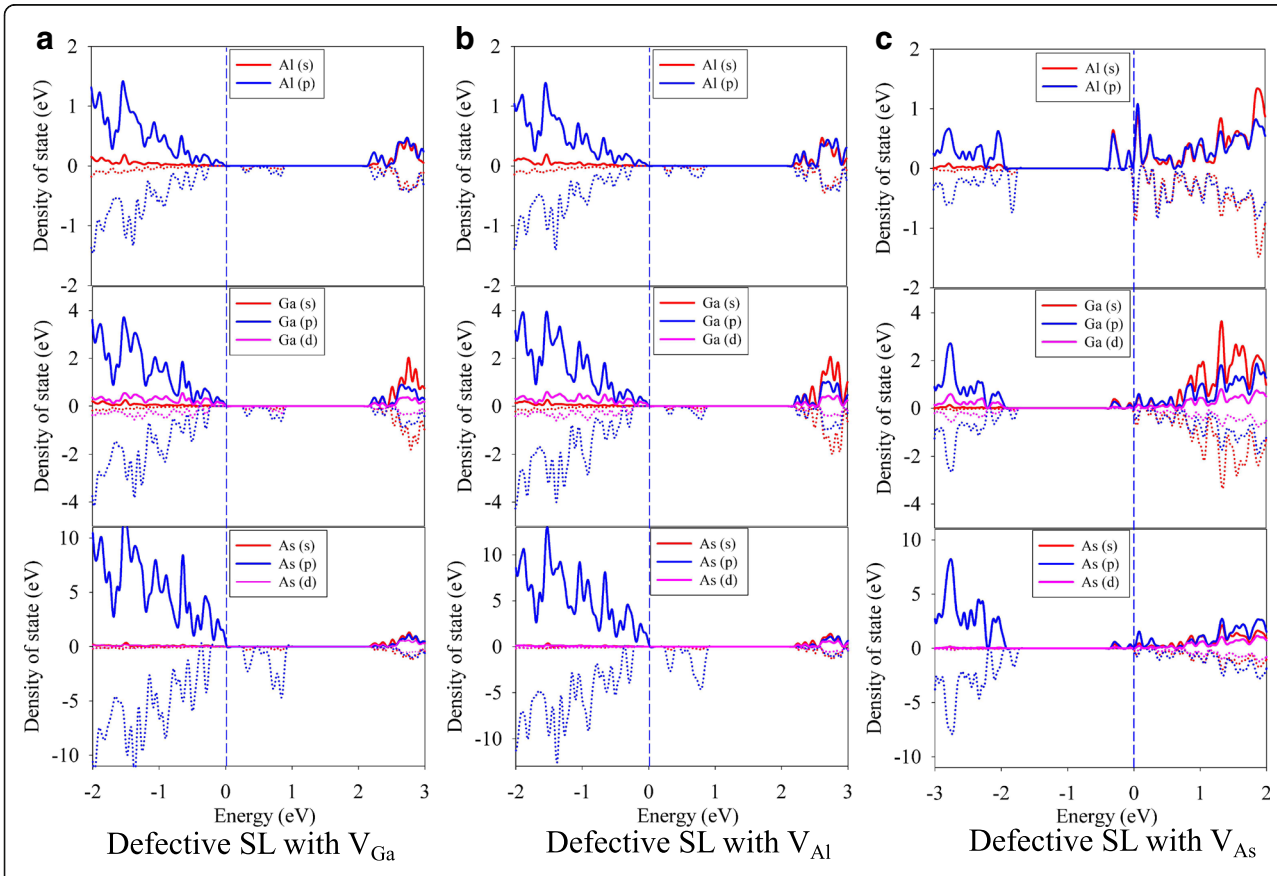

Fig. 8 The partial density of state of defective GaAs/AlAs superlattice with **a** V_{Ga}, **b** V_{Al} and **c** V_{As} vacancy defects. V_X (X = Ga, Al, or As) X vacancy

main influence of the group-III vacancies is on the *p* states. As shown in Fig. 7c, the band structure of the defective SL with V_{As} defect splits into spin-up and spin-down parts, and the defect levels appear near the conduction band. Since the V_{As} defect acts as an n-type dopant, the fermi level shifts to higher energy and crosses the defect level edge. Kahaly et al. have investigated the electrical properties of the GaAs-AlAs heterointerfaces and found that V_{As} defect at the interface lead to quasi 2-DEG [7], which is consistent with our results. Our calculations show that the vacancies have different effects on the band structure of GaAs/AlAs SL, i.e., the V_{As} defect induces metallicity of GaAs/AlAs SL, and the V_{Ga} and V_{Al} defects reduce the band gap of SL structure significantly.

The Effects of Interstitial Defects on the Band Structure of GaAs/AlAs Superlattice

Figure 9 presents the band structures of SL structure with interstitial defects. It is noted that the fermi level shifts to high energy and crosses the conduction band edge (see Fig. 9a and b), due to the fact that the group-III interstitials are donor-like defects. Consequently, the defective SLs with Ga_{int} and Al_{int} show metallic character. As shown in Fig. 9c, in the spin-up and spin-down parts of band structure, the impurity levels appear near the conduction band and the fermi level crosses the impurity level edge, indicating the induced metallicity of defective GaAs/AlAs SL with As_{int}. Obviously, the interstitial defects significantly change the electronic structures of GaAs/AlAs SL and generally induce metallicity of defective SL structure.

Comparing the band structures and representative PDOS of the GaAs/AlAs SL with antisites, vacancies, and interstitials, we find that the defects modify the electronic structures considerably, except the cases of Ga_{Al} and Al_{Ga} antisite defects. Besides, the band gap narrowing and even metallicity are induced, which will influence the performance of GaAs/AlAs SL drastically.

The Effects of Point Defects on the Electron Mobility of GaAs/AlAs Superlattice

The electron mobility at 0 K can be calculated from the equation $\mu = e\tau/m^*$, where e is the electron charge, τ is the relaxation time, and m^* is the effective mass of carrier [32]. The electron effective masses can be evaluated from the curvature of the band structures via the relation $m^* = \hbar^2\left(\frac{d^2\varepsilon}{dk^2}\right)^{-1}$ [32], where $\hbar$ is the reduced Planck constant, k is the wave vector, and ε is the energy of conduction band minimum. As shown in Fig. 4a and b, we obtain $m^* = 0.057\ m_e$ for GaAs and $m^* = 0.19\ m_e$ for AlAs, agreeing well with the experimental values of $0.057\ m_e$ for GaAs [33] and $0.124\ m_e$ for AlAs [34], where m_e is the static electron mass. The relaxation time for AlAs and GaAs is assumed to be 0.17 and 0.48 ps, respectively [35]. The electron mobility of GaAs and AlAs at 0 K are calculated to be $1.48 \times 10^4 cm^2/Vs$ and $1.57 \times 10^3\ cm^2/Vs$, respectively, which is comparable to the experimental values of $0.94 \times 10^4\ cm^2/Vs$ for GaAs [36] and $0.28 \times 10^3\ cm^2/Vs$ for AlAs [37].

As shown in Table 5, the electron effective mass at the Γ point (m^*_Γ) is determined to be $0.113\ m_e$ for the pristine GaAs/AlAs SL and the relaxation time τ is assumed to be 0.4 ps [38]. The electron mobility along the z direction, i.e., Γ-X direction in the Brillouin zone ($\mu_{\Gamma-X}$) is calculated to be $0.623 \times 10^4\ cm^2/Vs$ for ideal GaAs/

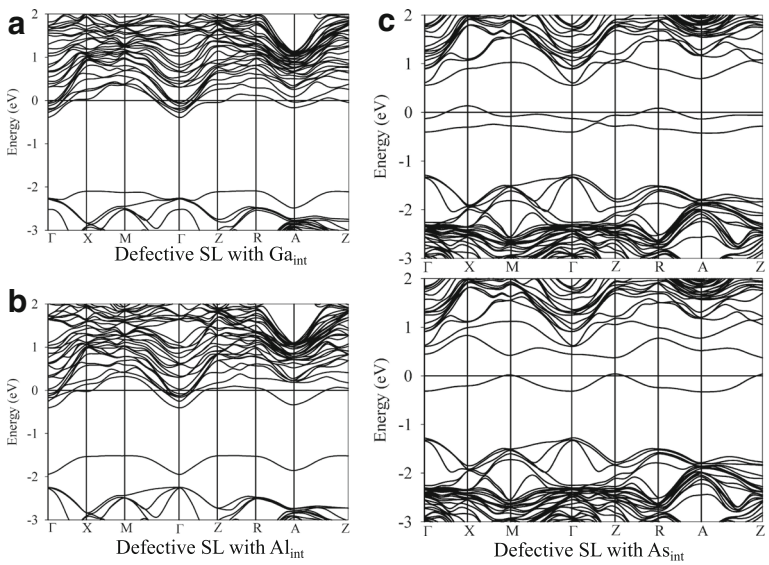

Fig. 9 The band structures of defective GaAs/AlAs superlattice with **a** Ga_{int} defect, **b** Al_{int} defect and **c** As_{int} defect. X_{int} (X = Ga, Al, or As) X interstitial

Table 5 The band gap, electron effective mass at the Γ point (m_Γ^*), and electron mobility along the z direction, i.e., Γ-X direction in the Brillouin zone ($\mu_{\Gamma-X}$) for defective GaAs/AlAs superlattice

Defect type	Band gap (eV)	Effective mass (m_Γ^*)	Electron mobility ($\mu_{\Gamma-X}$)
Ideal			
–	2.06	0.113 (0.07[a])	0.623 (1.0[a])
Antisite			
Ga_{Al}	1.98	0.124	0.567
Al_{Ga}	2.01	0.142	0.496
As_{Ga}	–	0.163	0.432
As_{Al}	–	0.119	0.591
Ga_{As}	0.1	0.267	0.263
Al_{As}	0.15	0.227	0.311
Interstitial			
Ga_{int}	–	0.313	0.225
Al_{int}	–	0.289	0.243
As_{int}	–	0.223	0.315
Vacancy			
V_{Ga}	0.47	0.729	0.097
V_{Al}	0.44	0.682	0.103

X_Y: (X, Y = Ga, Al, or As) X occupying the Y lattice site; V_X: X vacancy; X_{int}: X interstitial. m_Γ^* in the units of the static electron mass m_e; $\mu_{\Gamma-X}$ in the units of $10^4\ cm^2/Vs$. [a]Ref. [38]

AlAs SL, which is comparable to the experimental value of $1.0 \times 10^4\ cm^2/Vs$ [38]. As for the defective SL with antisite defects, the value of $\mu_{\Gamma-X}$ is comparable with that for the ideal SL, except for the cases of Ga_{As} and Al_{As} defects. The electron mobility along the Γ-X direction is determined to be $0.263 \times 10^4\ cm^2/Vs$ and $0.311 \times 10^4\ cm^2/Vs$ for Ga_{As} and Al_{As} defective states, respectively, which are much smaller than that for the ideal state. It is noted that the Ga_{int}, Al_{int} and As_{int} defects also reduce the electron mobility significantly, as indicated by the values of $0.225 \times 10^4\ cm^2/Vs$ for Ga_{int}, $0.243 \times 10^4\ cm^2/Vs$ for Al_{int} and $0.315 \times 10^4\ cm^2/Vs$ for As_{int}. As compared with antisite and interstitial defect, the vacancies have the most profound effects. For V_{Ga} and V_{Al} defects, the values of $\mu_{\Gamma-X}$ are about six times smaller than that of pristine state. The V_{As} defect also significantly decreases the electron mobility, as indicated by $0.127 \times 10^4\ cm^2/Vs$. Tanaka et al. have investigated the effects of electron irradiation on the electrical properties of GaAs/AlGaAs heterostructures and they found that the electron mobility was reduced at doses greater than $5 \times 10^{20}\ cm^{-2}$ [10]. Especially, the defect creation in GaAs channel region, rather than n-AlGaAs layer, is thought to be the main cause of the mobility degradation [10]. Recently, it has been suggested that the electrons are possibly trapped by defects or impurity and produce metastable states accompanied by lattice relaxation [39]. Consequently, the electronic structure and carrier mobility of GaAs/AlAs SL are influenced significantly by the point defects. Therefore, it is necessary to enhance the radiation tolerance of GaAs/AlAs SL to improve its electronic performance under radiation environment.

Conclusions

In this work, a hybrid density functional theory study is performed to investigate the effects of point defect on the electrical properties of GaAs/AlAs superlattice (SL). The calculated defect formation energies show that the antisite defects are the most favorable in bulk GaAs and AlAs. In GaAs/AlAs SL structure, the antisite defects are always dominant under cation-rich and As-rich conditions and the interstitial defects are very difficult to form during the whole range of chemical potentials. It is shown that the different point defects have various effects on the electronic structures of GaAs/AlAs SL. The As_X (X = Al or Ga) and X_{As} antisite defects always induce metallicity, although the defective SLs with X_{As} antisites show spin splitting. As for vacancies, the defective SL with V_{As} shows metallicity character, and the group III vacancy defects reduce the band gap of the superlattice significantly. The metallicity is also found in the defective GaAs/AlAs SL with the interstitial defects. The further carrier mobility calculations show that the interstitial and vacancy defects reduce the electron mobility significantly, while the antisite defects have relatively smaller influence.

Abbreviations

2-DEG: Two-dimensional electron gas; AIMD: *Ab initio* molecular dynamics; Al: Aluminum; AlAs: Aluminum arsenide; As: Arsenic; As_X: As occupying the X lattice site; DFT: Density functional theory; Ga: Gallium; GaAs: Gallium arsenide; HEMT: High electron mobility transistors; HSE: Heyd-Scuseria-Emzefhof; LED: Light-emitting diode; N: Nitrogen; PDOS: Partial density of state; QCLs: Quantum cascade lasers; SL: Superlattice; VASP: Vienna *Ab Initio* Simulation Package; V_X (X = Ga, Al or As): X vacancy; X_{As}: X occupying the As lattice site; X_{int}: X interstitial; Zn: Zinc

Acknowledgements

The theoretical calculations were performed using the supercomputer resources at TianHe-1 located at National Supercomputer Center in Tianjin.

Funding

Haiyan Xiao was supported by the NSAF Joint Foundation of China (Grant No.U1530129). Zijiang Liu was supported by National Natural Science Foundation of China (Grant No. 11464025) and the New Century Excellent Talents in University under Grant No. NECT-11-0906 and the Key Talent Foundation of Gansu Province.

Availability of Data and Materials

The datasets generated during and/or analyzed during the current study are available from the corresponding author on reasonable request.

Authors' Contributions

HX and XZ designed the calculations. MJ conducted the calculations and wrote the manuscript. SP, GY, ZL and LQ contributed the discussion and interpretation of the results. All authors read and approved the final manuscript.

Competing Interests

The authors declare that they have no competing interests.

Publisher's Note

Author details

[1]School of Physics, University of Electronic Science and Technology of China, Chengdu 610054, China. [2]Institute of Nuclear Physics and Chemistry, Chinese Academy of Engineering Physics, Mianyang 621900, China. [3]Department of Physics, Lanzhou City University, Lanzhou 730070, China.

Received: 28 June 2018 Accepted: 14 September 2018
Published online: 26 September 2018

References

1. Barkissy D, Nafidi A, Boutramine A, Charifi H, Elanique A, Massaq M (2016) Electronic properties of GaAs/AlAs nanostructure superlattice for near infrared devices at low temperatures. J Low Temp Phys 182:185–191
2. Botti S, Andreani LC (2001) Electronic states and optical properties of GaAs/AlAs and GaAs/vacuum superlattices by the linear combination of bulk bands method. Phys Rev B 63:235313
3. Botti S, Vast N, Reining L, Olevano V, Andreani LC (2004) Ab initio and semiempirical dielectric response of superlattices. Phys Rev B 70:045301
4. Fauzi DA, Rashid NKAM, Karim JA, Zin MRM, Hasbullah NF, Fareed AS (2013) Electrical performances of commercial GaN and GaAs based optoelectronics under neutron irradiation. In: 5th international conference on mechatronics, vol 53, p 012029
5. Ferhat M, Zaoui A, Certier M (1997) Electronic structure calculation for $(GaAs)_1(AlAs)_1$ monolayer superlattice. Phys Status Solidi B-Basic Res 204: 673–678
6. Hakkarainen T, Pavelescu EM, Arstila K, Dhaka VDS, Hakulinen T, Herda R, Konttinen J, Tkachenko N, Lemmetyinen H, Keinonen J (2005) Optical properties of ion irradiated and annealed InGaAs/GaAs quantum wells and semiconductor saturable absorber mirrors. J Phys D-Appl Phys 38:985–989
7. Kahaly MU, Nazir S, Schwingenschlogl U (2011) Band structure engineering and vacancy induced metallicity at the GaAs/AlAs interface. Appl Phys Lett 99:123501
8. Ribeiro M, Fonseca LRC, Ferreira LG (2011) First-principles calculation of the AlAs/GaAs interface band structure using a self-energy-corrected local density approximation. Epl 94:27001
9. Spasov S, Allison G, Patane A, Eaves L, Hopkinson M, Airey R (2006) Modifying the electronic properties of GaAs/AlAs superlattices with low-density nitrogen doping. J Appl Phys 100:063718
10. Tanaka N, Ishikawa T (1994) Energy-dependence and depth distribution of electron-beam-induced damage in GaAs/AlGaAs heterostructures. J Electron Mater 23:341–346
11. Zhang SB, Hybertsen MS, Cohen ML, Louie SG, Tomanek D (1989) Quasiparticle band gaps for ultrathin GaAs/AlAs(001) superlattices. Phys Rev Lett 63:1495–1498
12. Wang EG, Jin WM, ZLi Y, Wang HY (1990) Local electronic structures of the native defects in modulation-doped AlAs/GaAs superlattices. J Phys-Condes Matter 2:4405
13. Wang EG, Wang DS (1992) Native defects in a GaP_1/InP_1 strained-layer superlattice—local electronic-structure and diffusion mechanism. J Phys-Condes Matter 4:311–1321
14. Zollo G, Tarus J, Nieminen RM (2004) Reliability of analytical potentials for point-defect simulation in GaAs. J Phys-Condes Matter 16:3923–3932
15. Wang C, Zhang QM, Bernholc J (1992) Theory of Zn-enhanced disordering in GaAs/AlAs superlattices. Phys Rev Lett 69:3789–3792
16. Mitra S, Stark JP (1991) Role of vacancies and implantation defects in GaAs/AlAs superlattice intermixing. J Mater Sci 26:6650–6654
17. Jiang M, Xiao HY, Peng SM, Yang GX, Liu ZJ, Zu XT (2018) A comparative study of low energy radiation response of AlAs, GaAs and AlAs/GaAs superlattice and the damage effects on their electronic structures. Sci Rep 8:2012
18. Becke AD (1993) A new mixing of hartree-fock and local density-functional theories. J Chem Phys 98:1372–1377
19. Heyd J, Scuseria GE, Ernzerhof M (2003) Hybrid functionals based on a screened coulomb potential. J Chem Phys 118:8207–8215
20. Kresse G, Furthmüller J (1996) Efficient iterative schemes for ab initio total-energy calculations using a plane-wave basis set. Phys Rev B 54:11169–11186
21. Perdew JP, Burke K, Ernzerhof M (1996) Generalized gradient approximation made simple. Phys Rev Lett 77:3865–3868
22. Ahmed R, Hashemifar JS, Akbarzadeh H, Ahmed M, Fazale A (2007) Ab initio study of structural and electronic properties of iii-arsenide binary compounds. Comput Mater Sci 39:580–586
23. Mao Y, Liang XX, Zhao GJ, Song TL (2014) A lattice parameters and band structure of ternary mixed crystals $Al_xGa_{1-x}As$ from first-principle calculations. J Phys: Conf Ser 490:012172
24. Vivaldo Leiria C, Matteo JC (2010) Extended DFT+U+V method with on-site and inter-site electronic interactions. J Phys-Condes Matter 22:055602
25. Liu Y, Jiang Y, Zhou R, Feng J (2014) First principles study the stability and mechanical properties of MC (M=Ti, V, Zr, Nb, Hf and Ta) compounds. J Alloy Compd 582:500–504
26. Vurgaftman I, Meyer JR, Ram-Mohan LR (2001) Band parameters for III-V compound semiconductors and their alloys. J Appl Phys 89:5815–5875
27. Filippi C, Singh DJ, Umrigar CJ (1994) All-electron local-density and generalized-gradient calculations of the structural properties of semiconductors. Phys Rev B 50:14947–14951
28. Posselt M, Gao F, Weber WJ, Belko V (2004) A comparative study of the structure and energetics of elementary defects in 3C- and 4H-SiC. J Phys-Condes Matter 16:1307
29. Aslı Ç, Cem S, Ceyhun B (2014) Strained band edge characteristics from hybrid density functional theory and empirical pseudopotentials: GaAs, GaSb, InAs and InSb. J Phys D-Appl Phys 49:085104
30. Kobayashi N, Toriyama T, Horikoshi Y (1987) Resonant raman effect in thin-layered AlAs/GaAs superlattices. Appl Phys Lett 50:1811–1813
31. Dehghanzadeh M, Ahmadian F (2017) Half-metallicity and magnetism of the full-heusler compounds KYX_2 (Y=Ti, V, and Cr; X=C, N and O). Solid State Commun 251:50–59
32. Nazir S, Upadhyay Kahaly M, Schwingenschlögl U (2012) High mobility of the strongly confined hole gas in AgTaO3/SrTiO3. Appl Phys Lett 100:201607
33. Nakwaski W (1995) Effective masses of electrons and heavy holes in GaAs, InAs, AlAs and their ternary compounds. Physica B 210:1–25
34. Dumke WP, Lorenz MR, Pettit GD (1972) Enhanced indirect optical absorption in AlAs and GaP. Phys Rev B 5:2978–2985
35. Gonzalez B, Palankovski V, Kosina H, Hernandez A, Selberherr S (1999) An energy relaxation time model for device simulation. Solid State Electron 43: 1791–1795

36. Stillman GE, Wolfe CM, Dimmock JO (1970) Hall coefficient factor for polar mode scattering in n-type GaAs. J Phys Chem Solids 31:1199–1204
37. Ettenberg AGSM, Dreeben A, Gilbert SL (1971) Vapor growth and properties of AlAs. J Electrochem Soc 118:1355–1358
38. Kusters RM, Wittekamp FA, Singleton J, Perenboom JAAJ, Jones GAC, Ritchie DA, Frost JEF, André JP (1992) Electron relaxation times in high-carrier-density gaas-(ga, al)as heterojunctions. Phys Rev B 46:10207–10214
39. Nakai Y, Hattori K, Okano A, Itoh N, Haglund RF (1991) Nonthermal laser sputtering from solid surfaces. Nucl Instrum Meth B 58:452–462
40. Ghebouli MA, Choutri H, Bouarissa N, Ghebouli B (2012) First-principles study on stability, energy gaps, optical phonon and related parameters of $In_{1-x-y}Al_xGa_yAs$ alloys. J Solid State Chem 192:161–167
41. Camargo-Martinez JA, Baquero R (2013) The band gap problem: the accuracy of the wien2k code confronted. Rev Mex Fis 59:453–459